Forschung im Ingenieurwesen (2023) 87:1129–1136
https://doi.org/10.1007/s10010-023-00713-3

ORIGINALARBEITEN/ORIGINALS

Experimental investigation of moving contact pattern in helical planetary gearboxes

Marius Fürst[1] · Sebastian Sepp[1] · Daniel Schweigert[1] · Michael Otto[1] · Karsten Stahl[1]

Received: 26 March 2023 / Accepted: 22 August 2023 / Published online: 5 September 2023

Abstract

Planetary gear sets combine the characteristics of high-power density and compact design which are beneficial for a wide range of high-performance applications. Embedded in the efforts for resource efficiency and cost reduction, new challenges arise regarding a lightweight design. An accurate prediction of the load sharing on the individual planetary gears and especially of the load distribution of the meshing gears is of major importance. A uniform load distribution enables the design of the individual tooth meshes without load increases and oversizing. However, a varying load distribution has been observed in planetary gearboxes with respect to the rotation of the carrier which is caused by misaligned central shafts of the gearbox. This behavior is influenced by several factors, such as manufacturing and assembly deviations, the rigidity of shafts, housing and bearings, the number of planets, the quality of the gear wheels and the operating conditions. To determine the exact load distribution, detailed simulations or extensive experimental prototype tests are required. In an early design phase, these detailed boundary conditions are not yet defined and their effect on a moving contact pattern therefore cannot be reliably considered.

Thus, in this paper an experimental investigation of the influencing factors on a varying load distribution with regard to the carrier rotation is presented. Based on experimental data recommendations for the design of planetary gearboxes are derived.

✉ Marius Fürst
marius.fuerst@tum.de

[1] School of Engineering and Design, Department of Mechanical Engineering, Gear Research Center (FZG), Technical University of Munich, Boltzmannstraße 15, 85748 Garching near Munich, Germany

Experimentelle Untersuchung zum Tragbildwandern in schrägverzahnten Planetengetrieben

Zusammenfassung

Planetengetriebe zeichnen sich durch eine hohe Leistungsdichte und kompakte Bauweise aus, weshalb diese in einer Vielzahl an Hochleistungsanwendungen eingesetzt werden. Eingebettet in das Bestreben nach Ressourceneffizienz und Kostenreduzierung ergeben sich in einer Konstruktion in Leichtbauweise neue, zusätzliche Herausforderungen. Von großer Bedeutung ist eine genaue Vorhersage der Lastaufteilung auf die einzelnen Planetenräder und insbesondere der Lastverteilung in den Zahneingriffen der kämmenden Räder. Eine gleichmäßige Lastverteilung ermöglicht die Auslegung der Verzahnungen ohne die Notwendigkeit der Berücksichtigung zusätzlicher Lastüberhöhungen und folglich ohne Überdimensionierung. Bei Planetengetrieben wurde jedoch eine veränderliche Lastverteilung in Abhängigkeit der Umlaufstellung des Planetenträgers beobachtet, welche mitunter durch nichtfluchtende Zentralwellen des Getriebes verursacht wird. Dieses Verhalten wird von mehreren Faktoren beeinflusst, wie Herstellungs- und Montageabweichungen, der Steifigkeit von Wellen, Gehäuse und Lagern, der Anzahl der Planeten, der Qualität der Zahnräder und den Betriebsbedingungen. Um die genaue Lastverteilung ermitteln zu können, sind aufwändige Simulationen oder umfangreiche experimentelle Prototypentests erforderlich. In einer frühen Entwurfsphase sind diese detaillierten Randbedingungen noch nicht definiert und die Auswirkung auf ein Wandern des Tragbildes während eines Umlaufes des Planetenträgers kann daher nicht zuverlässig adressiert werden.

In dieser Arbeit wird eine experimentelle Untersuchung von Einflussfaktoren auf eine veränderliche Lastverteilung in Bezug auf die Umlaufstellung des Planetenträgers vorgestellt. Aus den experimentellen Daten werden Empfehlungen für die Auslegung von Planetengetrieben abgeleitet.

1 Introduction

In comparison to standard helical gearboxes, planetary gear sets have a more complex structure. However, their various advantages, such as high-power density, coaxial central shaft alignment and high gear ratios, promote their wide usage in diverse applications. In general, a uniform load distribution in the tooth contacts and an equal load sharing between the planets is essential to fully utilize the load capacity potential. Any gearbox built must cope with the limited manufacturing accuracy and assembly deviations by which the performance is affected. In the design process, unequal load sharing and the non-uniformity of the load distribution can be considered by load factors in the load carrying capacity assessment, e.g. ISO 6336 [1].

Theoretical and experimental studies extensively evaluated the behavior and influencing factors on planetary load sharing and load distribution. Singh [2] derived a physical explanation for the load sharing behavior considering the number of planets, positional errors and floating shaft systems. For the characterization of static and dynamic load sharing behavior in dependency of the planet number and manufacturing deviations, several experimental studies were conducted, focusing on the measurement by using strain gauges: Ligata [3], Hidaka [4], Kahraman [5, 6], Singh [7] (root-strain based) and Boguski [8], Hayashi [9], Götz [10] (planet pin-strain based). The aforementioned did not investigate the load distribution along the tooth face width. To do so, multiple strain gauges must be applied in a single tooth root along the width. Such measurements are covered in Nam [11], Leimann [12], Kamps [13], Terrin [14] and Brecher [15]. For a wind turbine gearbox, Kamps [13] and Leimann [12] observed a variation of the load distribution in dependency of the carrier rotational position. For a final drive with strain gauges applied at the sun gear, Terrin [14] identified a change of strain distribution within one rotation of the sun. In the latter two studies, a variable face load factor was found, however it is not mentioned whether this was due to a systematic effect. Brecher [15] investigated the influence of shaft misalignments in a wind turbine gearbox and identified a dependency of the load distribution and tooth root stresses on the carrier position.

As outlined, experimental studies on the effect of a moving contact pattern in dependency of the carrier rotational position are scarce. However, it is essential to address this effect as early as the preliminary design phase of the gearbox since it affects the load carrying capacity of the gears. The present study therefore experimentally investigates the impact of carrier shaft misalignment on the tooth contact of a three-planet planetary gear set.

2 Test rig

In the present study, measurements were conducted at a planetary gearbox with a static load applied on the gears. In particular, the test rig itself is designed to fit onto a coordinate measuring machine (CMM) to capture the elastic deformation behavior of the gearboxes' shafts, outer bearing rings and gears. The working principle and the rig instrumentation are explained in the following. Further

information on the rig and gear design process is covered in [16–18].

2.1 Principle

In the power path of the test rig, there is a worm gear which is used to apply the load to the sun shaft of the planetary gear set, see Fig. 1. The planetary gear set has a fixed ring gear and the carrier acts as the output shaft. Its basic design specifications are listed in Table 1. The carrier shaft is connected to a tensioning device which provides the supporting moment equivalent to the fourfold of the input torque. A torsion spring is integrated in the tensioning device to allow the displacement of the central shafts during the loading process of the gearbox. The load is ramped up over a certain angle of rotation, thus allowing the shafts to turn and locate within the bearing clearances. To accurately set the mesh position, the struts of the tensioning device can be fixed at an arbitrary rotational angle. When the rotatable struts, which are connected to the carrier, get in contact with the fixed struts of the tensioning device, the load can be further increased up to the intended test torque value.

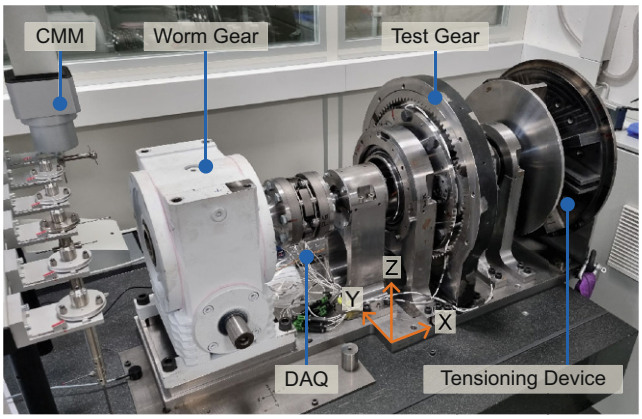

Fig. 1 Planetary gear test rig

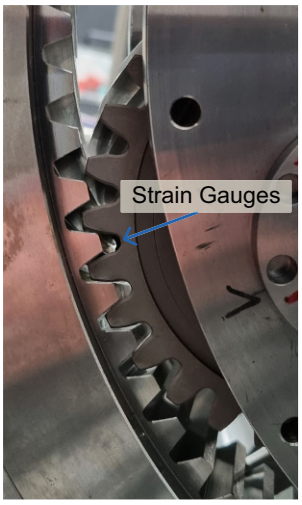

Fig. 2 Loaded gear teeth of planet and ring gear mesh

Table 1 Test rig specification

Stationary gear ratio	i_{12}	= −3.0
Gear ratio	i_{1c}	= 4.0
Max. input torque	M_1	= 1800 Nm

Table 2 Coordinate measuring machine

Model	Leitz Reference 600	
Probing accuracy [19]	δ_{CMM}	= 0.9 µm
Ambient temperature	T	= 20.0°C

Since the purpose of this study is to identify the impact of shaft misalignments on the tooth contact, the rig can be equipped with eccentric sleeves at the bearing seats. By misaligning the outer bearing rings of the shaft, the shaft itself is shifted, too. In the same manner, the planet pins can be misaligned by assembling eccentric sleeves in the carrier pinholes. The planetary gear set conducted in this study is shown in Fig. 1.

Figure 2 shows the loaded gear teeth of the meshing planet and ring gear. Here, the meshing position is set such that the contact line at one tooth of the planet gear largely covers the tooth width. The corresponding tooth root is equipped with five strain gauges to measure the tooth root strains. These are equidistantly spaced and attached to the surface by means of an adhesive bond. The tooth root equipped with the strain gauges is highlighted in Fig. 2.

2.2 Coordinate measuring machine

With a CMM, precise measurements of geometric shapes and spatial positions are feasible. The main characteristics of the institute's CMM are summarized in Table 2.

It is installed in an air-conditioned laboratory to minimize the influence of thermal expansion on the measurement results. Through a regular calibration of the measuring tips, the accuracy of the measurements is ensured. This process is performed by using a high-precision reference sphere, see Fig. 3. The measured values at various positions

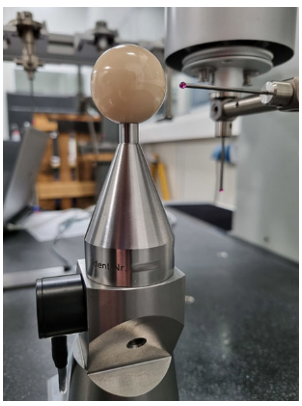

Fig. 3 Reference sphere with temperature sensor for measuring tip calibration

on the surface of the sphere are compared with theoretically ideal values and, if necessary, the machine and evaluation parameters are adjusted accordingly.

3 Test gears and test matrix

The experiments in this investigation were carried out on a planetary gear set with helical gears. These are case hardened (sun and planet), respectively hardened and tempered (ring gear). The geometry data of the test gear is specified in Table 3.

For a uniform load distribution at 50% of the maximum design load, standard flank modifications are used [16–18]. In principle, any carrier rotational angle of the gearbox can be set, and the deformation can be measured with the CMM, i.e. the planet and gear mesh position is unconstrained. However, each measurement is a time-consuming task and therefore a limitation to three representative carrier positions was required, see Fig. 4.

The teeth numbers of the gears have been tuned so that meshing occurs on a specific planet gear tooth again when the carrier is rotated by increments of 120°. Planet gear 1 is applied with strain gauges, therefore the subsequently used definition of the three carrier rotational positions uses the rotation angle of planet 1 to the positive Y-axis in mathematical negative direction (counter clockwise) as a reference.

The elastic deformation behavior under different loads is investigated in five load levels. For this, the load was increased starting at low loads up to the target load (loading). Then, the load was gradually reduced from a slightly higher load to the target load (relieving). With this procedure, the influence of tooth friction forces on the deformation can be assessed. The load levels are defined in Table 4 and reference the torque at the sun shaft/gear of the planetary gear set. The torque was measured and monitored during the tests with a calibrated strain gauge application on the shaft.

All individual gearbox configurations, i.e. variations in shaft misalignments, have been measured in the specified three carrier rotational positions and the five load levels. The configurations in scope of this investigation are summarized in Table 5.

Table 3 Test gear data

Helix angle	β	= 21.3°
Normal module	m_n	= 4.2 mm
Contact ratio (S/P)	ε_α	= 1.205
Contact ratio (P/R)	ε_α	= 1.229
Overlap ratio	ε_β	= 1.101
Center distance	a	= 135.0 mm
Common face width	b	= 40.0 mm

Table 4 Load levels

Level	Sun torque	Load direction
L1	M = 0 Nm	–
L2	M = 450 Nm	Loading
L3	M = 900 Nm	Loading
L4	M = 900 Nm	Relieving
L5	M = 450 Nm	Relieving

Table 5 Test setups with specification of shaft misalignment (eccentricity of bearing seat sleeves)

Setup	Carrier (input)	Direction	Carrier (output)	Direction
S1	–	–	–	–
S2	100 µm	Y+	–	–

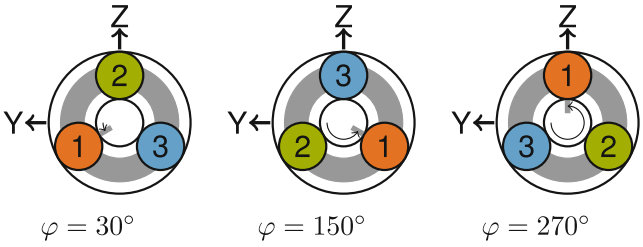

Fig. 4 Carrier rotational positions and planet gear formation

4 Data evaluation

Since a single measurement takes several minutes, the boundary conditions on the system differ slightly during this period even if the investigation is of static nature. This is due to creeping, i.e., the slow deformation of the material and the part connections subject to mechanical stresses. Therefore, strain measurements at the tooth root have been performed multiple times during the test run. First, the arithmetic mean $x_{\varepsilon,i}$ of the captured discrete-time signal is calculated, see Eq. 1. f_s is the sampling frequency, i.e. the recorded number of samples per second, and t is the recording time.

$$x_{\varepsilon,i} = \frac{1}{f_s \cdot t} \cdot \sum_{k=1}^{n(t)} x_{\varepsilon,i,k} \tag{1}$$

A weighted mean value $\overline{x}_{\varepsilon,j}$ of all measurement series is calculated for every strain gauge j. The weighted mean of all series $\overline{x}_{\varepsilon,j}$ is calculated according to Eq. 2:

$$\overline{x}_{\varepsilon,j} = \frac{\sum_{i=1}^{n} w_i \cdot x_{\varepsilon,i}}{\sum_{i=1}^{n} w_i} \tag{2}$$

In this formula, $x_{\varepsilon,i}$ denotes the arithmetic mean of the discrete-time signal of series i and w_i is the associated

weight. The weights w_i are chosen as the inverse proportion to the variance σ_i^2 of the mean $x_{\varepsilon,i}$, see Eq. 3:

$$w_i = \frac{1}{\sigma_i^2} \tag{3}$$

The course of the tooth root strain along the face width is then given by the mean strains of the strain gauges at their five discretized supporting points.

5 Results

Figure 5 illustrates the tooth root strains along the tooth width for setups S1 and S2.

As outlined previously, it is the weighted mean $\overline{x}_{\varepsilon,j}$ of several measurement series at the discrete supporting points in the tooth root, which is shown for load levels L2–L5 representing the course of the strains along the tooth width. The values are given for the three carrier rotational positions φ as specified in Fig. 4. Since exclusively planet 1 is equipped with strain gauges, the results refer to this gear.

The measured strains at the supporting points show a change in magnitude along the tooth width. This behavior is expected due to the inclined orientation of the contact line in a helical gear mesh since, amongst others, the lever between the tooth root and the point of application of the tooth force is variable along the tooth width. As a reference, an example of the simulated tooth root stresses along the field of action for a helical gear is given in Fig. 6.

The interpolated curves between the measured strain values at the supporting points, see Fig. 5, show a clear change also in dependency of the carrier position. For the experiments, the discrete carrier positions measured have been set up using an inclinometer at the tensioning device to allow for reproducible boundary conditions in all configurations. Given that, the striking difference between the position $\varphi = 270°$ and the remaining two positions already in the nominal non-misaligned setup S1 will be explained during this analysis. For the carrier position $\varphi = 270°$ the measurements show only small strains on the right portion of the tooth width. However, the measured strain on the leftmost strain gauge only differs slightly between the three carrier positions. The derivatives of the interpolated strain curves even indicate a higher strain present at the left tooth edge for carrier position $\varphi = 270°$. Due to this fact, a moving of the strain distribution and in consequence of the load distribution along the tooth width in dependency of the carrier rotational position is monitored and experimentally confirmed.

The described trend is qualitatively similar for both setups S1 and S2, however, the measured strains show differences in quantity, see Fig. 7.

The differences are related to the purposely misaligned bearing seats of the carrier shaft, see Table 5. In setup S2, the carrier is tilted in the X-Y-plane which propagates to the tooth contact of planet and ring gear. For the carrier position $\varphi = 270°$, the tilting appears mostly as a skewing of the mating tooth flanks. If an ideal, completely solid assembly, would be shifted this way, planet gear 1 would approach its mating ring gear flank closely at the left flank edge whereas the right flank edge would be retracted. With the measured strains to increase at the left side of the flank in setup S2, see Fig. 7, the expected behavior is confirmed.

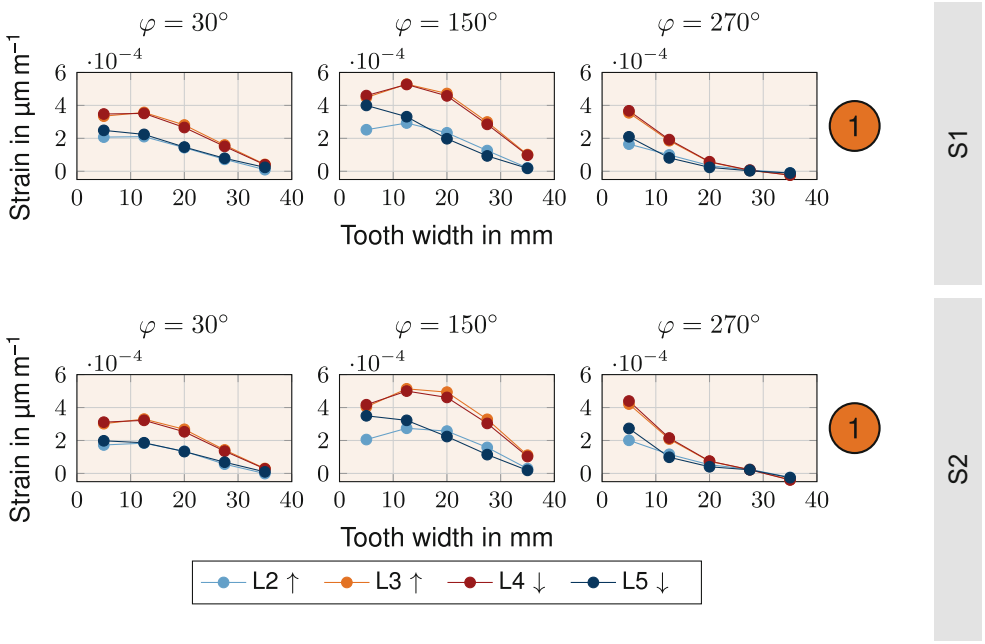

Fig. 5 Tooth root strain along the planet tooth width for setup S1 (*top*) and S2 (*bottom*) at different load levels, planet and ring gear mesh

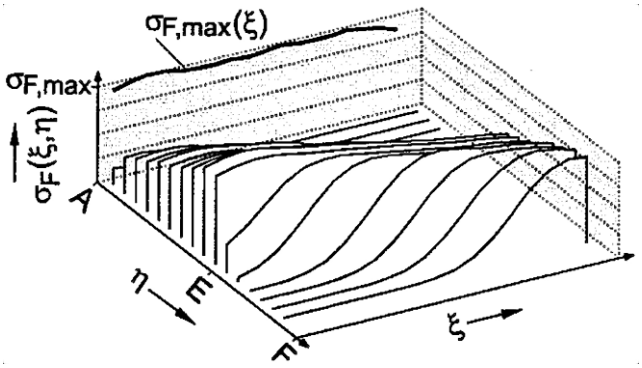

Fig. 6 Tooth root stresses of a helical gear: $\beta = 20°$, $\varepsilon_\alpha = 1.2$, $\varepsilon_\beta = 1.0$ [20]

At the same time, the measured strains in the remaining positions show a decrease in magnitude at the left, emphasizing the presence of a moving contact pattern with respect to the carrier rotation in planetary gearboxes.

In addition to the strain measurements, the deflection of the central shafts was captured with the CMM. Figure 8 shows the results of the shaft center point measurements and the linear interpolations of the points which are related to the different shafts. In the diagrams, the measurements of the absolute positions are drawn and given in the two coordinates Y and Z, as specified in Fig. 1. It is the sun shaft on the left, the ring gear in the middle and the carrier shaft ranging from the middle to the right. For the ring gear, the two outside points represent the limits of the gear width and are extrapolated from the central midpoint and the measured gear face plane.

With the load increased, a change in the deflections due to elastic deformation can be observed. For the deflection in Z-direction (X-Z-plane), a good alignment of all shafts is present since the interpolated shaft midlines are in good conformance to a common line. In Y-direction (X-Y-plane), the deflections are of higher magnitude and do not follow a common line.

In no-load condition (L1), the differences in Y-deflections are comparatively small, however, they increase significantly with higher loads. These findings demonstrate a non-negligible influence of the elastic casing deformation on the shaft misalignment due to the induced loads. This taken into consideration, it explains that there is a limited difference between the strain distributions when purposely tilting the carrier shaft from setup S1 to S2, see Fig. 5. However, by tilting the carrier in negative direction around the positive Z-axis (setup S2), the expectation that, for exam-

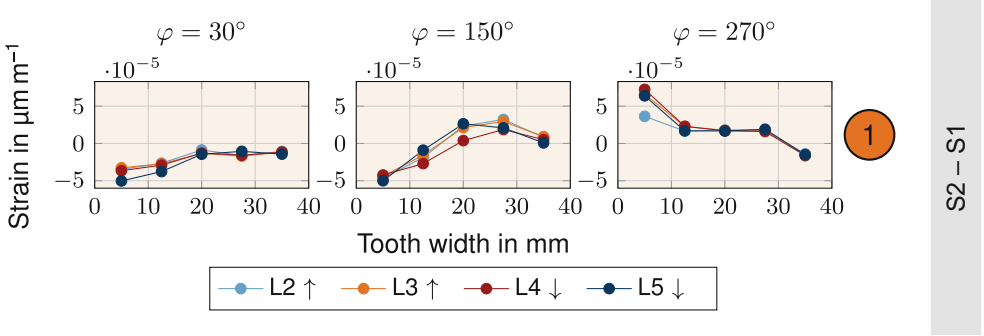

Fig. 7 Difference of the tooth root strain along the planet tooth width of setups S1 and S2 at different load levels, planet and ring gear mesh

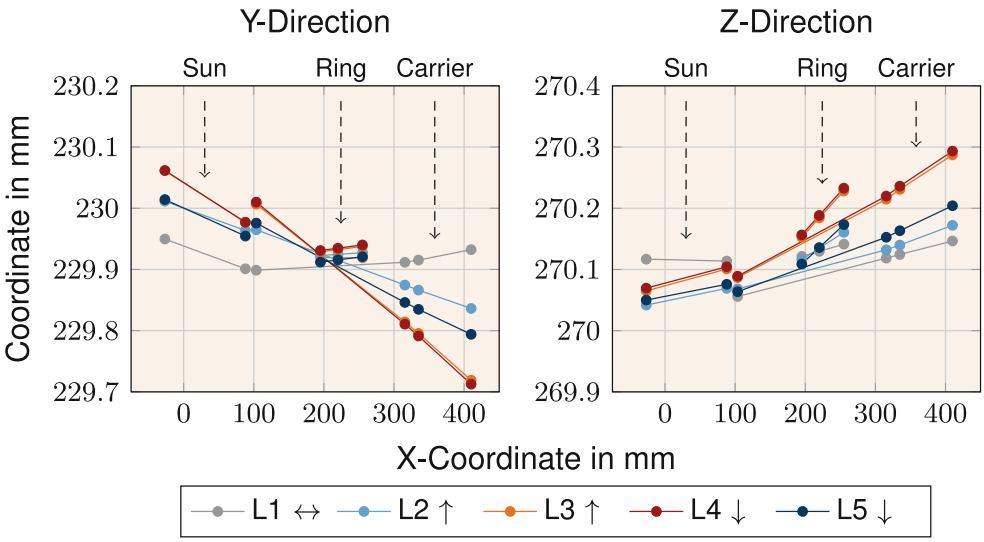

Fig. 8 Shaft center coordinates at the probing points for setup S1 at different load levels

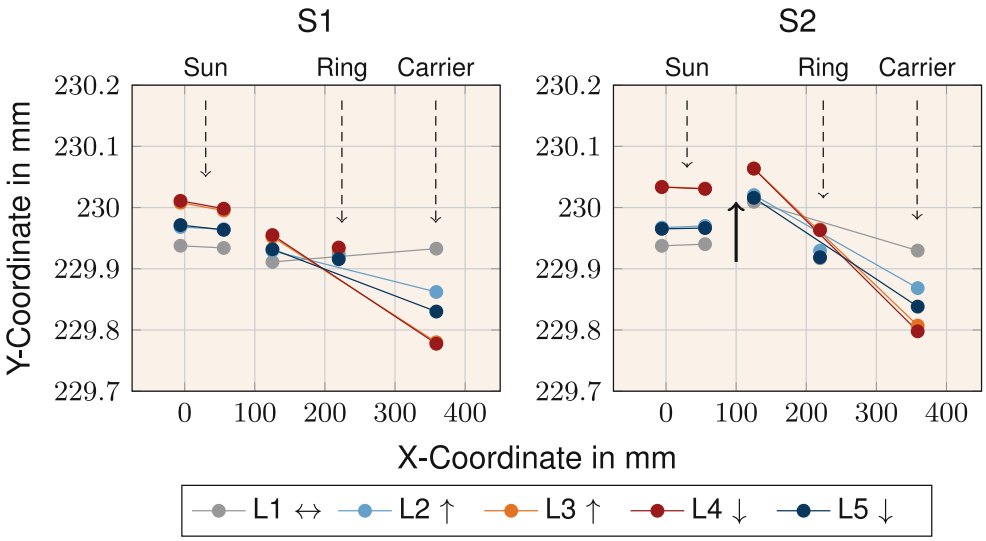

Fig. 9 Bearing seat center coordinates at the probing points for setup S1 (*left*) and S2 (*right*) at different load levels, misalignment by eccentric sleeve indicated with *bold arrow*

ple for the carrier position $\varphi = 270°$, the load concentrates to the left, is clearly visible. When meshing with the ring gear, the left flanks are loaded at the planet gears. Therefore, the superimposed carrier tilting leads to a relief of the right flank edge and thus shifting the load further to the left. The same consideration is analogously valid for the other carrier positions.

The tilting of the carrier is achieved by eccentric sleeves at the bearing seats. The effect of the nominal value of eccentricity on the shaft deflection is weakened by the bearing clearances and manufacturing tolerances. Figure 9 shows the midpoints of the sleeves, measured through three probing points at their outer diameter surfaces for setups S1 and S2. In both setups, no modifications were carried out at the sun shaft bearings and the fixed ring gear mount. Therefore, the center point coordinates are in good agreement. However, at the carrier bearing seats, the effect of the purposely misaligned centers is clearly identifiable and highlighted in Fig. 9. It is this misalignment imposed on the carrier shaft that leads to varying conditions in the tooth contact in dependency of the carrier rotational position, as it was previously shown and analyzed. In gearbox design, it is recommended to assess whether the applied loads or the selected manufacturing tolerances can cause similar displacement of the shafts. In this case, the effect on the tooth contact in terms of load distribution should be precisely analyzed and adequately considered in the gear(box) design.

6 Conclusion

In this paper, the impact of shaft misalignments on the tooth contact was experimentally investigated on a three-planet helical planetary gear set. Based on a strain measurement in the planet tooth root, the effect of the purposely altered boundary conditions on the strain distribution along the tooth width was monitored. Furthermore, the deformation behavior of the gearbox was measured by a coordinate measuring machine to capture the deflection and orientation of the central shafts. By taking the carrier rotational position into consideration, the following observations are obtained for the tooth contact of planet and ring gear:

The strain distribution in the tooth root along the tooth width of the planet gear may vary if the carrier and ring gear are misaligned. In turn, the load distribution is affected in accordance which results in higher, but also shifting stresses on the tooth flank (moving contact pattern). If external non-torque loads are acting, e.g. on the carrier shaft, which might cause the misalignment, tight bearing clearances could be beneficial to limit the shifting of the contact pattern and in turn positively impact the load sharing behavior, as it was shown by Guo [21]. In addition, a flexible ring gear might be an option to mitigate the remaining misalignment of the tooth flanks if the ring gear can adapt to the unequal distribution of the tooth mesh forces over the circumference.

The deformation behavior of the casing under load may lead to a deflection of the central shaft bearing seats and should be carefully considered.

Acknowledgements The presented results are based on the research project IGF no. 20796 N/l undertaken by the Research Association for Drive Technology e. V. (FVA); supported partly by the FVA and through the German Federation of Industrial Research Associations e. V. (AiF) in the framework of the Industrial Collective Research Programme (IGF) by the Federal Ministry for Economic Affairs and Climate Action (BMWK) based on a decision taken by the German Bundestag. The authors would like to thank for the sponsorship and support received from the FVA, AiF and the members of the project committee.

Funding Open Access funding enabled and organized by Projekt DEAL.

Conflict of interest M. Fürst, S. Sepp, D. Schweigert, M. Otto and K. Stahl declarethat they have no competing interests.

References

1. ISO 6336-1:2019-11: Calculation of load capacity of spur and helical gears—Part 1: Basic principles, introduction and general influence factors, 2019.
2. Singh A (2010) Load sharing behavior in epicyclic gears: Physical explanation and generalized formulation. Mech Mach Theory 45:511–530
3. Ligata H, Kahraman A, Singh A (2008) An experimental study of the influence of manufacturing errors on the planetary gear stresses and planet load sharing. J Mech Des 130(4):41701-1–041701-9. https://doi.org/10.1115/1.2885194
4. Hidaka T, Terauchi Y (1976) Dynamic behavior of planetary gear : 1st report load distribution in planetary gear. Bull JSME 19:690–698
5. Kahraman A, Ligata H, Singh A (2010) Influence of ring gear rim thickness on planetary gear set behavior. J Mech Des. https://doi.org/10.1115/1.4000699
6. Kahraman A (1999) Static load sharing characteristics of transmission planetary gear sets: model and experiment. SAE Trans 108:1954–1963
7. Singh A, Kahraman A, Ligata H (2008) Internal gear strains and load sharing in planetary transmissions: model and experiments. J Mech Des 130(7):072602-1–072602-10. https://doi.org/10.1115/1.2890110
8. Boguski B, Kahraman A, Nishino T (2012) A new method to measure planet load sharing and sun gear radial orbit of planetary gear sets. J Mech Des 134(7):071002-1–071002-8. https://doi.org/10.1115/1.4006827
9. Hayashi T, Li XY, Hayashi I, Endo K, Watanabe W (1986) Measurement and some discussions on dynamic load sharing in planetary gears. Bull JSME 29:2290–2297
10. Götz J, Siglmüller F, Fürst M, Otto M, Stahl K (2022) Experimental investigation of the dynamic load sharing of planetary gearboxes. Forsch Ingenieurwes 86:295–302
11. Nam JS, Park YJ, Han JW, Nam YY, Lee GH (2016) The effects of non-torque loads on a three-point suspension gearbox for wind turbines. Int J Energy Res 40:618–631
12. Leimann D (2013) Evolution in gear micro-geometry design for wind turbine gearboxes with respect to load distribution and noise and vibrations. In International Conference on Gears. VDI Wissensforum
13. Kamps A, Klein-Hitpass A (2015) Einfluss von elastischen Verformungen auf die Auslegung und den Betrieb von Getrieben für Windkraftanlagen. In: DMK – Dresdner Maschinenelemente Kolloquium
14. Terrin A, Libardoni M, Meneghetti G (2018) Experimental analysis of tooth-root strains in a sun gear of the final drive for an off-highway axle. Procedia Struct Integr 8:276–287
15. Brecher C, Löpenhaus C, Theling J (2020) Influence of planet carrier misalignments on the operational behavior of planetary gearboxes. Gear Technol 37:46–55
16. Fingerle A, Otto M, Stahl K (2020) Definition of a coefficient to evaluate a moving contact pattern in planetary gearboxes. Forsch Ingenieurwes 84:235–243
17. Fürst M, Fingerle A, Otto M, Stahl K (2023) Experimentelle Untersuchungen zu Einflussfaktoren auf das Tragbildwandern in Planetengetrieben: Schlussbericht zu IGF-Vorhaben Nr. 20796 N/I. Technische Universität, München
18. Fingerle A, Otto M, Stahl K (2020) FVA-Nr. 592 III – Validierung RIKOR III: Validierung der Verformungsrechnung in RIKOR – Detaillierte Betrachtung gekoppelter Getriebesysteme. Forschungsvereinigung Antriebstechnik e. V., Frankfurt am Main
19. Hexagon Metrology (2006) Betriebsanleitung Leitz Reference 600.
20. Schinagl S (2002) Zahnfußtragfähigkeit schrägverzahnter Stirnräder unter Berücksichtigung der Lastverteilung, Dissertation, Technische Universität München.
21. Guo Y, Keller J, LaCava W (2015) Planetary gear load sharing of wind turbine drivetrains subjected to non-torque loads. Wind Energ 18:757–768